Quaternary Research (2024), **122**, 143–158
doi:10.1017/qua.2024.26

Research Article

The relevance of biotic processes on modern tufa deposits, with an example from the Bonito region, Central-West Brazil

Jéssica Thaís Ferreira Oste, Almério Barros França, Leonardo Fadel Cury and Anelize Manuela Bahniuk

Laboratory of Minerals and Rocks Analysis (LAMIR), Federal University of Paraná, Curitiba, PR, Brazil

Abstract

Tufas are freshwater carbonate rocks that form in continental environments through a combination of physical, chemical, and biological processes. This study investigates the role of microorganisms in the precipitation of Quaternary tufa deposits in the Serra da Bodoquena Formation, in the Bonito region. Two sites along the Mimoso River, named Taíka and Mimosa, characterized by the pool–barrage–cascade depositional subenvironment, were selected for this study. Four distinct facies were identified: stromatolitic boundstones, phytoherm boundstones of algae, phytoherm boundstones of bryophytes, and phytoclastic rudstones. These facies were observed in diverse hydrological settings, including fast-flowing waters, such as waterfalls and cascades, as well as slow-flowing areas, such as pools and dams. The $\delta^{18}O$ depletion indicated a meteoric origin for the fluid involved in carbonate precipitation. The low $\delta^{13}C$ values were attributed to photosynthetic processes and the contribution of light carbon-enriched groundwater. The presence of *Oocardium stratum* and calcified organic mucilage from extracellular polymeric substance (EPS) corroborates the significant role of microorganisms in tufa formation, particularly in stromatolitic boundstones and phytoherm boundstones of algae. Rapid CO_2 degassing significantly contributes to mineralization in fast-flowing waters. Micro-CT results offer detailed insights into the relationship between mechanical processes and biological influences in shaping porosity characteristics. The findings of this study significantly enhance our understanding of the role of microorganisms in tufa formation, highlighting the complex interplay between biotic and abiotic processes in the development of different tufa facies. Moreover, the insights gained from this study provide valuable implications for interpreting tufa deposits worldwide.

Keywords: Tufas, Quaternary, Serra da Bodoquena, Stromatolites, Carbonatic facies

Introduction

Tufas are freshwater carbonate deposits that form in karstic areas through a combination of abiotic (CO_2 outgassing) and biotic (microorganisms' metabolisms, trapping and binding) processes (Ford and Pedley, 1996; Arenas-Abad et al., 2010; Gradziński, 2010), the latter playing a significant role in carbonate precipitation (Shiraishi et al., 2008a, 2017; Dupraz et al., 2009; Arp et al., 2010; Pedley, 2014). These deposits are characterized by the precipitation of $CaCO_3$ from bicarbonate-rich fluids, often accompanied by CO_2 outgassing, particularly during changes in substrate gradient or increased fluid flow velocity (Merz-Preiβ and Riding, 1999; Andrews and Brasier, 2005; Capezzuoli et al., 2014).

Microbial activity has been widely documented as a component for the deposition of carbonate rocks, ranging from the early stages of Earth's history to modern water systems that exhibit carbonate deposition (Riding, 2000). Microorganisms, particularly prokaryotic cells from the Bacteria domain and certain eukaryotes, are responsible for carbonate precipitation in various environments, including marine and lacustrine systems, fluvial tufa, travertines, and speleothems (Riding, 1991, 2000). Understanding the biotic processes involved in tufa formation has significant implications for biogeochemical cycles, paleoenvironmental records, and for possible microbial carbonate analogues (Andrews, 2006; Pedley et al., 2009; Arenas et al., 2014a; Shiraishi et al., 2017).

Microorganisms play a significant role in tufa formation through various mechanisms. One such mechanism involves the secretion of extracellular polymeric substances (EPS) by microorganisms, which act as nucleation sites for mineral formation (Merz-Preiβ and Riding, 1999; Riding, 2000; Shiraishi et al., 2008a; Dupraz et al., 2009; Pedley et al., 2009). Additionally, photosynthetic processes carried out by cyanobacteria and algae can induce carbonate disequilibrium by absorbing CO_2 from the water, leading to an increase in pH and subsequent enhancement of CO_3 saturation (Arp et al., 2001; Shiraishi et al., 2010; Shiraishi, 2011).

The present study focuses on the Bonito region at Mato Grosso do Sul State, Brazil, which presents recent and inactive tufa deposits of Quaternary age. The tufas in this region are predominantly found along rivers, creeks, and abandoned meanders within the karstic system of the Corumbá Group. The Bonito region offers a unique opportunity to investigate these continental freshwater deposits. While recent works in the same region have provided valuable insights into tufa facies and their environmental forming conditions (Oste et al., 2021), as well as early diagenetic changes in these recent tufa deposits (Oste et al., 2023), the primary focus of the present study is to unravel the role of microorganisms in tufa formation. Specifically, we aim to investigate how the

Corresponding author: Jéssica Thaís Ferreira Oste; Email: jessica.oste@gmail.com
Cite this article: Oste JTF, França AB, Cury LF, Bahniuk AM (2024). The relevance of biotic processes on modern tufa deposits, with an example from the Bonito region, Central-West Brazil. *Quaternary Research* **122**, 143–158. https://doi.org/10.1017/qua.2024.26

biogenic nature of tufa deposits influences the different facies and porosity arrangements.

Geological Setting

Located southwest of the Pantanal wetlands in the State of Mato Grosso do Sul (Brazil), the Serra da Bodoquena Hill (Fig. 1), up to 800 meters high, extends for 200 km in the north–south direction. The Serra da Bodoquena, within the Paraguai Fold Belt, is part of the Bodoquena Plateau and composed of a set of north–south trending mountains (Sallun Filho et al., 2009a). The Paraguai Fold Belt is a Brazilian–Panafrican tectonic unit, bordering the Amazon craton and the Rio Apa block (Boggiani and Alvarenga, 2004; Campanha et al., 2011). Stratigraphically, this tectonic unit is subdivided into three other units: the lowermost part, formed by glaciogenic turbidites of the Cuiabá Group and Puga Formation; carbonates of the Araras and Corumbá groups; and siliciclastic rocks of the Alto Paraguai Group (Alvarenga and Trompette, 1993; Riccomini et al., 2007).

The Corumbá Group (Ediacaran Age) is subdivided into four units, including siliciclastic rocks at the bottom, followed by dolostones (Bocaina Formation), carbonate mudstones and limestones (Tamengo Formation), and lutites at the top (Almeida, 1965; Boggiani et al., 1993; Romero et al., 2016). Carbonate rocks from the Corumbá Group (Bocaina and Tamengo formations) are of great relevance because they are the source of $CaCO_3$ for the modern tufa development (Sallun Filho, 2005).

The tufas belonging to the Serra da Bodoquena system, are spread along rivers and creeks covering an erosive and angular unconformity with the underlying rocks of the Corumbá Group (Boggiani et al., 2002; Sallun Filho et al., 2009a, b; Oliveira et al., 2017). These tufa deposits have been informally included in the Pleistocene–Holocene Serra da Bodoquena Formation, which is subdivided into two members: the Rio Formoso Member and the Fazenda São Geraldo Member (Sallun Filho et al., 2009a; Oliveira et al., 2017). Elements such as cascades and barrier tufas of the Rio Formoso Member, either active or not, occur exclusively in river channels (Sallun Filho et al., 2009a). Shells of gastropods and ostracodes are common, along with Characeae algae (green macro algae) or mosses, leaves. and branch fragments encrusted by carbonate (Boggiani et al., 2002). Unconsolidated micritic mud deposits from the Fazenda São Geraldo Member occur in ancient wetlands, lakes, and abandoned meanders (Boggiani et al., 2002; Sallun Filho et al., 2009a), with ostracodes and microgastropods (Utida et al., 2012, 2017). In this study, we characterize the tufa deposits as discontinuous calcareous bodies and unconsolidated sediment, exhibiting limited distribution and no lateral continuity, despite the proposal of a stratigraphic unit encompassing them.

The climate of the study area is considered as humid tropical, with little difference in precipitation and temperature, which falls under the Aw category of the Köppen–Geiger classification. Mean air temperature is 23.8°C, with 1–3 dry months (June to August), also with the lowest temperatures. Annual precipitation (1684 mm) occurs mostly in December and January (https://pt.climate-data.org [accessed 14 October 2024]), which also corresponds to the months with highest temperatures.

Materials and Methods

Two sites, named Taika (21°00′24.1″S, 56°29′58.7″W) and Mimosa (21°00′00.1″S, 56°30′40″W and 20°59′58.9″S, 56° 30′40.4″W), have been chosen for the present study. They are located along the Mimoso River near the city of Bonito, in Mato Grosso do Sul State, Brazil (Fig. 1). Oste et al. (2021, 2023) previously investigated tufa deposits along the Mimoso River, however, our present work is focused on distinct fresh outcrops of waterfalls and pools–barrage–cascade subenvironments. Sampling was conducted during the dry season, at the end of autumn–winter period, in August and September of 2015 and 2016.

The depositional environment of active tufa precipitation was characterized during field campaigns, during which 25 samples were collected for laboratory analysis at the Laboratório de Análises de Minerais e Rochas (LAMIR), Universidade Federal do Paraná. Petrographic analysis included both mesoscopic and microscopic descriptions using handheld lenses and a petrographic microscope (Axio Zeiss Imager A.2) linked to a camera (AxioCam MRc) for image captures. Twelve thin sections were described. For lithological descriptions, the Dunham (1962) classification, modified by Embry and Klovan (1971), as well as studies by Arenas-Abad et al. (2010) and Gradziński et al. (2013), were followed. Additional petrographic studies and porosity analysis were conducted using a SkyScan X-ray 1172 microtomograph (90kV potential; 112 µA current, 12.8 µm/pixel resolution and 2000×1336 camera resolution) for 3D imaging of 10 sample cubes with a volume of 1 cm^3. Porosity determination was optimized through binarization processes specific to each sample. The Choquette and Pray (1970) classification was used for the porosity description. Additionally, six samples were analyzed using a scanning electron microscope (SEM) (JEOL JSM-6010LA model). The microscopic and microtomography analyses were conducted at LAMIR, Federal University of Paraná.

X-ray diffraction (XRD) analyses were performed on 25 powdered samples using a PANalytical diffractometer (EMPYREAN model) with a copper anode (Cu Kα1 = 1.5406 Å) at a Theta × 2Theta geometry, operating at 40 kV and 30 mA. Identification and percentages of the mineral phases (error of ± 5%) were estimated by using X'Pert High Score Plus software (PDF-2 database) and applying the RIR (reference intensity ratio) method for semi-quantitative analysis. A PANalytical X-ray fluorescence spectrometer (AXIOS MAX model, SuperQ 5.3 software) was used to analyze 10 major oxides and 4 trace elements, as well as for conducting LOI (lost on ignition) analysis on the same 25 powdered and dried samples. Isotopic bulk analyses of $\delta^{13}C$ and $\delta^{18}O$ were performed on 25 powdered samples, which were dissolved in 100% anhydrous phosphoric acid. The CO_2 was extracted using a GasBench II system and IRMS Delta V Advantage mass spectrometer (Thermo Fisher Scientific). The isotopic values are expressed in δ notation in parts per thousand (‰) relative to the VPDB (Vienna Peedee Belemnite) standard. Analytical precision is 0.04‰ for $\delta^{13}C$ and 0.08‰ for $\delta^{18}O$. Geochemical, mineralogical and isotopic analyses were conducted at LAMIR, at the Federal University of Paraná (UFPR).

Results

The Northern part of Bonito city is characterized by the predominance of active and inactive tufas of the Rio Formoso Member, forming several-meter high waterfalls and dam–pool–cascade subenvironments, along rivers and creeks, in a stepped fluvial profile. For this study, we focused exclusively on outcrops along the Mimoso River, specifically at two sites: Taíka and Mimosa (Fig. 1). The Taíka site consists of small cascades and natural

https://doi.org/10.1017/qua.2024.26 Published online by Cambridge University Press

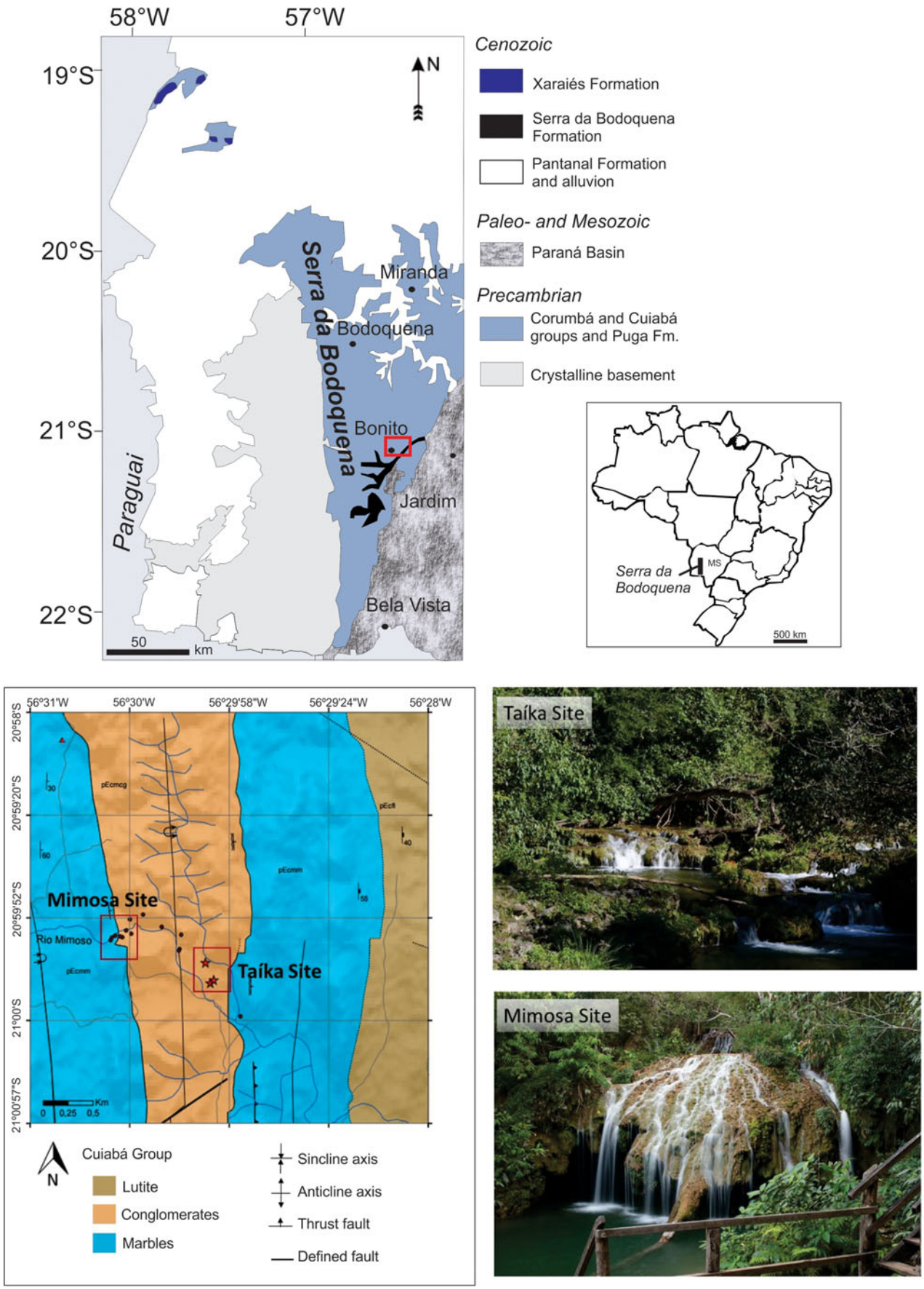

Figure 1. Geographic and geological settings of the study area. Taíka (21°00′24.1″S, 56°29′58.7″W) and Mimosa (21°00′00.1″S, 56°30′40″W and 20°59′58.9″S, 56° 30′40.4″W) sites highlighted by red squares. Modified from Campanha et al. (2011).

https://doi.org/10.1017/qua.2024.26 Published online by Cambridge University Press

dams extending approximately 10–20 m, while the Mimosa site features waterfalls measuring ~3–5 m high, smaller cascades, and dams spanning ~10 m in length.

Tufa facies: stromatolitic boundstones

The stromatolitic boundstones occur as laminated tufa or conical structures with irregular laminae, both in small cascades and dams (Fig. 2A–D). The lamination is well defined, consisting of alternating dark- and light-colored layers that are millimeters thick. Internally, the light-beige laminae are thinner and primarily composed of micrite, while the darker layers are porous and formed by micritic fibro-radiated filaments.

Microscopically, the stromatolitic boundstones are characterized by planar to gently domed lamination. The laminae are irregular and marked by an intercalation of: (1) dark and thin micritic laminae with a thickness of 1–3 mm; (2) clear spar crystals; (3) peloidal and highly porous micrite lamina 2–4 mm thick, and (4) elongated calcified filaments of cyanobacteria and/or algae, formed by a micritic nucleus encrusted with spar crystals (Fig. 2E and F). There are three types of pores observed in the stromatolitic boundstones: fenestral porosity, characterized by elongated pores aligned parallel to the lamination; growth-framework porosity, which is related to pores between calcified filaments; and moldic porosity, related to empty tubes formed after the decay of algae cells.

The stromatolitic tufa displays alternating undulating laminations, resulting in semi-radial microstructures observed through SEM imaging (Fig. 2G). These structures exhibit an oval shape with a diameter of approximately 100 µm and form bush-like structures with radiated calcified tubes (Fig. 2H). These tubes, with a diameter of 10 µm, are composed of stacked trigonal calcitic subcrystals, likely related to *Oocardium stratum* cells. Extracellular polymeric filaments are commonly present between radii-fibers, although no bacterial cell remains have been detected. Occasionally, the EPS appears as honeycomb-like networks.

Stromatolitic boundstones interpretation

The stromatolitic boundstones occur in various conditions, including fast-flowing areas, such as cascades or low-slope zones, and calm fluvial areas (Arenas-Abad et al., 2010; Gradziński et al., 2013; Arenas et al., 2014b; Berrendero et al., 2016). Typically, stromatolitic boundstones are formed by the rapid precipitation of calcite caused by mechanical CO_2 outgassing and microbial activity (Shiraishi et al., 2008b, Gradziński, 2010; Arenas and Jones, 2017). The laminated structure of stromatolites (alternating porous and denser laminae) is often associated with seasonal changes in physicochemical conditions and/or microbial communities (Kano et al., 2003; Shiraishi et al., 2008b; Arenas and Jones, 2017). In this study area, Oste et al. (2021) concluded that these stromatolites are directly associated with the seasonality of rain in the region.

Tufa facies: phytoherm boundstones of algae filaments

The phytoherm facies is characterized by fibro-radiated structures associated with algal filaments (Fig. 3A). This facies develops as mats in pools and ponded areas. The calcified filaments are displayed parallel to each other, with a brushy aspect (Fig. 3B) and can reach up to 2 cm in length. Typically, this facies consists of stacked algal mats, forming irregular and non-planar layers. Microscopically, these structures mainly comprise micritic filaments, with 0.2 mm in diameter, calcified by microspar to clear spar crystals (Fig. 3C and D) in a micritic matrix. Growth framework porosity predominates between the calcified filaments, usually 1–2 cm, and moldic porosity related to empty tubes.

SEM images revealed the presence of triangular domains of dendritic calcite as an early stage of crystal formation. The dendritic calcite grows in three regular directions and forms clusters of small microcrystal triads (Fig. 3E). These fiber microcrystals collectively create a triangular domain shape associated with EPS. The dendritic calcite forms a crust around the filaments, exhibiting partial dissolution at the center when viewed from the top, which results in circular moldic pores. This dissolution is likely associated with the consumption of organic content within filamentous cyanobacteria. Occasionally, the triangular domains of calcite develop into rhombs and euhedral crystals (Fig. 3F). The EPS displays filamentous structures related to the triangular domains of dendritic calcite, and no visible bacterial cells were preserved.

Phytoherm boundstones of algae filaments interpretation

Ponded and dammed areas, with slow-flowing or stagnant waters, create favorable conditions for the preservation of algae and microbial mats. This facies is characterized by the presence of vertical or inclined bushes of algae that align parallel to the flow direction (Arenas-Abad et al., 2010).

Tufa facies: phytoherm boundstones of bryophytes

The phytoherm facies is characterized by the presence of spongy calcified mosses, which have small leaves up to 1 cm in size. The bryophyte cushions occur near small cascades, in splash areas, or in dams with intermittent water flow (Fig. 4A and B). Microscopically, this facies exhibits a highly porous micritic matrix with moss leaves, whether preserved or not, coated by unclear microspar crystals (Fig. 4C). Large and empty moldic pores are commonly observed, occasionally containing remnants of organic matter.

SEM images show a cushion of living moss partially covered by filaments (Fig. 4D). Communities of pennate diatoms are attached to the moss leaves (Fig. 4E), interlocking with calcite crusts and encrusting diatoms. In the boundstones of bryophytes, the EPS may appear as a thin veneer (Fig. 4F) covering the moss leaves, incorporating diatoms frustules and calcite microcrystals. It is common to find fungal filaments inhabiting the bryophyte leaves.

Phytoherm boundstones of bryophytes interpretation:

Tufa environments, including the upper parts of barriers and dams with thin water laminae, offer favorable conditions for the growth of bryophytes, which thrive in well-lit areas. The calcitic crystals precipitated around the bryophyte leaves occur due to splashing and spraying of supersaturated water (Arenas et al., 2010; Arenas-Abad et al., 2010; Gradziński et al., 2013), or due to a temporary increase in water flow.

Tufa facies: phytoclastic rudstones

Phytoclastic rudstones occur at the tops of dams and cascades (Fig. 5A and B). They consist of plant fragments, such as leaves and small branches, covered by a thin calcitic crust and embedded in a micritic matrix (Fig. 5C). Gentle millimeter-thick laminations formed by oriented phytoclasts of leaves parallel to the flow can be observed.

https://doi.org/10.1017/qua.2024.26 Published online by Cambridge University Press

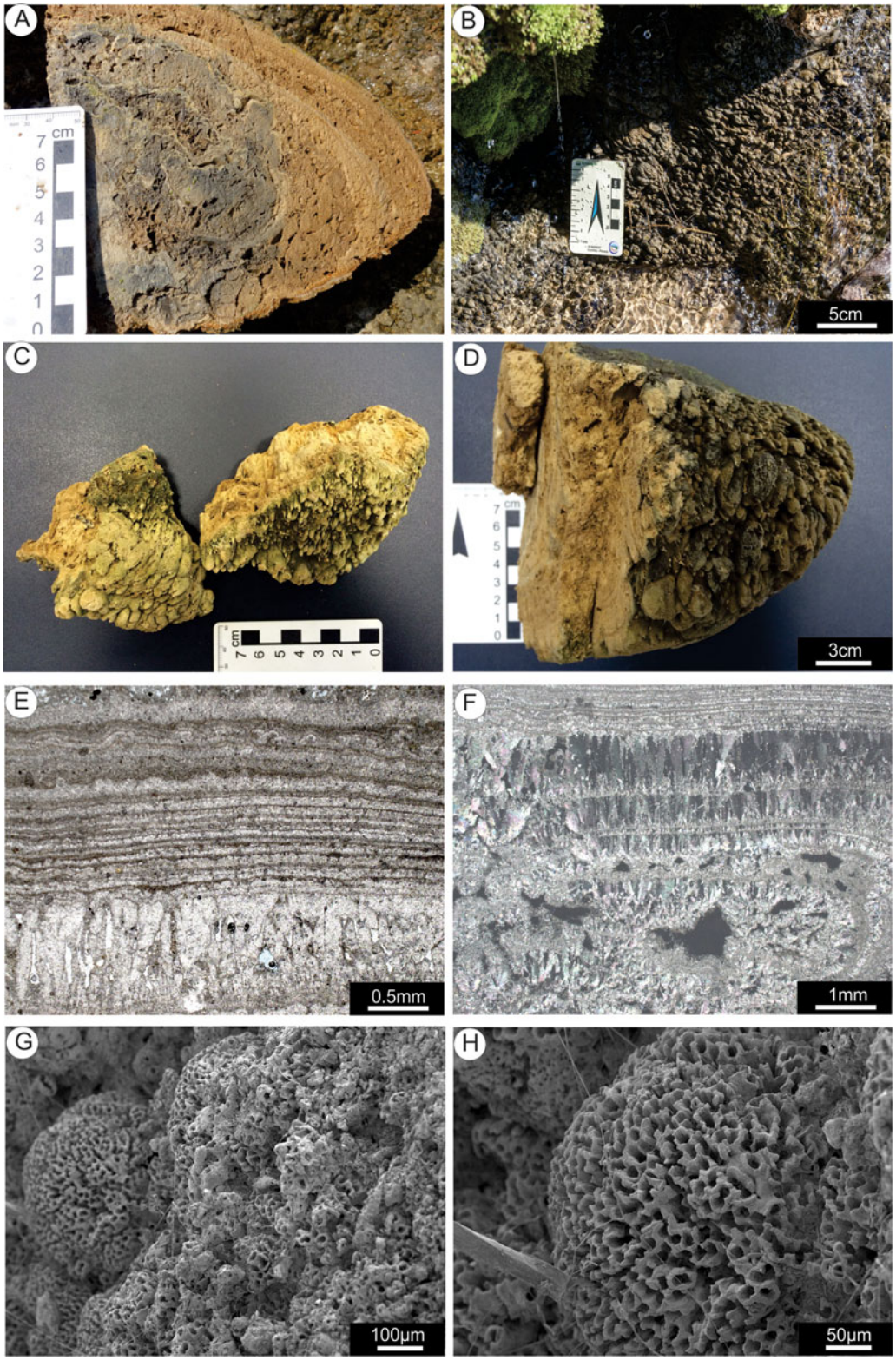

Figure 2. Stromatolitic boundstone. (A) Stromatolitic tufa characterized by well-defined laminations. (B) A small cascade with slow-flowing water. (C) Small conical features are common at the surface of laminated tufa. (D) Sample of stromatolitic tufa with greenish conical structures at the top. (E) Microscope image; lamination of stromatolitic boundstone, with dark and thin micritic laminae, microspar to spar laminae, and thick lamina with clear spar shrub-like crystals; parallel polarizers. (F) Microscope image; lamination of stromatolitic boundstone with thick laminae with shrub-like spar crystals; crossed polarizers. (G) SEM image; semi-radial micro-structures with oval shape. (H) SEM image; semi-radial calcified tubes.

https://doi.org/10.1017/qua.2024.26 Published online by Cambridge University Press

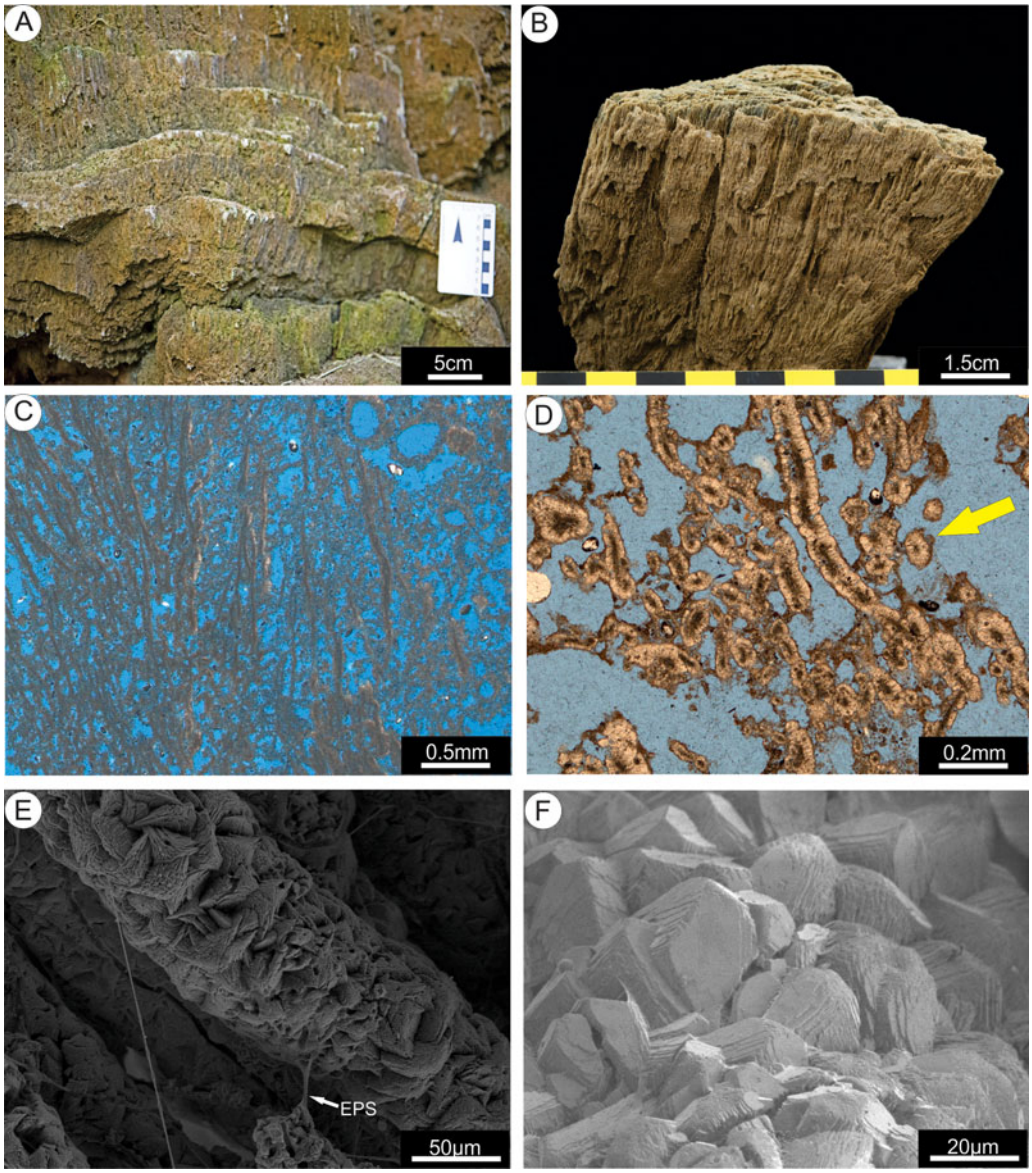

Figure 3. Phytoherm boundstone of algae. (A) Non-planar layers of fibro-radiated structures. (B) Sample of phytoherm boundstone of algae with calcified filaments. (C) Microscope image; micritic filaments with semi-parallel orientation and a micritic matrix. (D) Microscope image; filaments calcified with microspar to small clear spar crystals; circular shapes with micritic nuclei represent perpendicular cuts of filaments (yellow arrow). (E) SEM image; dendritic calcite forming triangular domains associated with EPS. (F) SEM image; rhomboidal and euhedral crystals formed by triangular domains of calcite.

Under microscopic examination, the phytoclasts are covered by a thin layer of dark micrite, occasionally grading to unclear microspar crystals or clear shrub-like spar crystals (Fig. 5D and E). The phytoclasts are often associated with calcified filaments of cyanobacteria or algae. The matrix primarily consists of dark, loose, and occasionally peloidal micrite. Moldic pores are related to phytoclasts, which typically retain a very thin remnant of organic matter (Fig. 5D).

In SEM images, phytoclastic rudstones reveal plant stalks with diameters of approximately 25 µm that are completely covered by calcite (Fig. 5F), with relatively low mucilage content (EPS). Phytoclasts (e.g. leaves and fragments of branches) appeared calcified by small crystals of micrite and/or microspar. Algal and/or cyanobacterial tubes are frequently present (Fig. 5F). Thin filaments (5–10 µm in diameter) connected to leaves and stalks are probably related to fungi.

Phytoclastic rudstones interpretation

Plant fragments can be transported from vegetated areas by flash floods, high velocity water flow (Gradziński et al., 2013), and/or be carried by wind. While erosion might occur during high-energy episodes, deposition of this facies occurs on tops of barriers or in dammed conditions (Arenas-Abad et al., 2010; Vázquez-Urbez et al., 2012) where micrite encrustation takes place in slow-flowing water.

Porosity analysis

Stromatolites, phytoherm boundstones, and phytoclastic rudstones generally have high values of total porosity in µ-CT analysis (Fig. 6A). The tomographic images for different sections within the tufa samples exhibit a porous morphology (Fig. 6B–E).

Moldic, growth framework and fenestral pores are considered selective types of porosity (Choquette and Pray, 1970).

https://doi.org/10.1017/qua.2024.26 Published online by Cambridge University Press

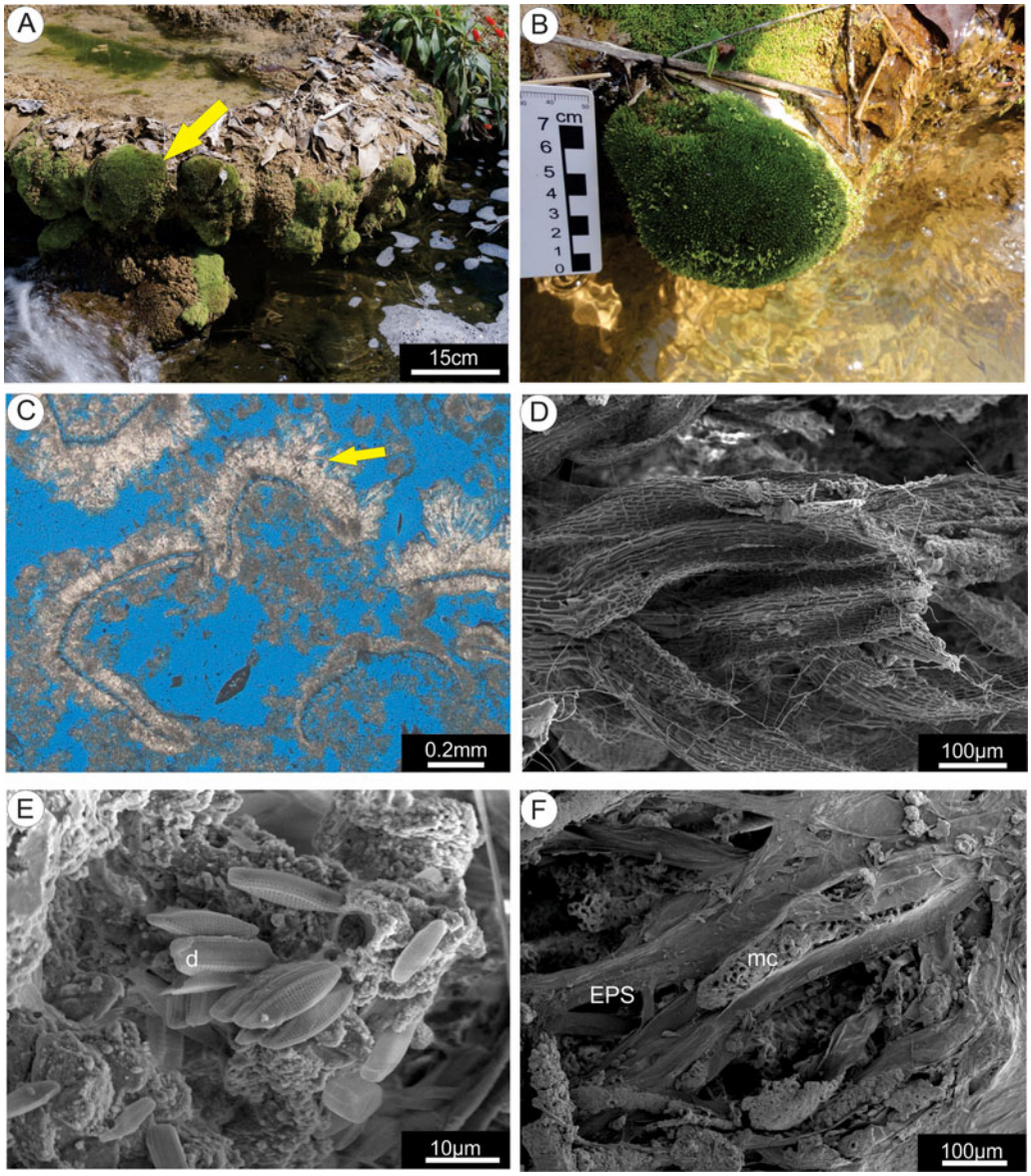

Figure 4. Phytoherm boundstone of bryophyte. (A) Dams formed by bryophyte cushions (yellow arrow) in a splash-water area. (B) Bryophyte cushion. (C) Microscope image; leaves of moss covered by clear shrub-like spar crystals (yellow arrow) in a micritic matrix. (D) SEM image; moss leaf with with thin fungal filaments and some disperse micritic crystals. (E) SEM image; pennate diatoms (d) associated with micritic crystals. (F) SEM image; veneer of EPS covering living moss with micrite (mc).

Moldic porosity, the most common type in the tufas of Bonito, is formed by the oxidation of organic matter of phytoclasts (Fig. 6D), gastropod shells, moss leaves, and algal filaments. Growth framework pores are commonly observed between calcified filaments of cyanobacteria and/or algae in phytoherm boundstones of algae (Fig. 6C) and stromatolitic boundstones (Fig. 6B). These pores are vertical and can reach up to 1 cm in size, similar to the radii-fibers. Fenestral porosity, a primary type of pore, occurs parallel to the lamination in stromatolitic boundstones (Fig. 6B). This type of porosity is characterized by isolated and elongated pores, with dimensions of up to 0.1 cm in the vertical axis and 1 cm in the horizontal axis. Interparticle and intercrystalline porosities, also considered selective types (Choquette and Pray, 1970), occur in all described facies, although they are not exclusive to a particular tufa facies.

X-ray microtomography revealed the highest porosities in phytoherm boundstones of bryophytes (Fig. 6E) and phytoclastic facies (Fig. 6D), with values of 66.32% and 43.80%, respectively (Table 1, Fig. 6A). The percentage of isolated pores was used as a parameter to indirectly analyze connectivity, with higher values indicating lower connectivity. The phytoclastic facies also exhibited the lowest values for isolated pores. In contrast, stromatolitic tufas and phytoherm boundstones of algae had the lowest total porosity rates, averaging 14%, due to their denser fabric.

It was possible to distinguish the internal part of moldic pores within phytoclasts from the radiated features on phytoherm boundstones of algae. The stromatolite facies exhibited some lamination and had pore sizes larger than the detection capacity of the equipment. The phytoclastic framework was typically chaotic, with no preferential direction of pores, most of which were not connected.

https://doi.org/10.1017/qua.2024.26 Published online by Cambridge University Press

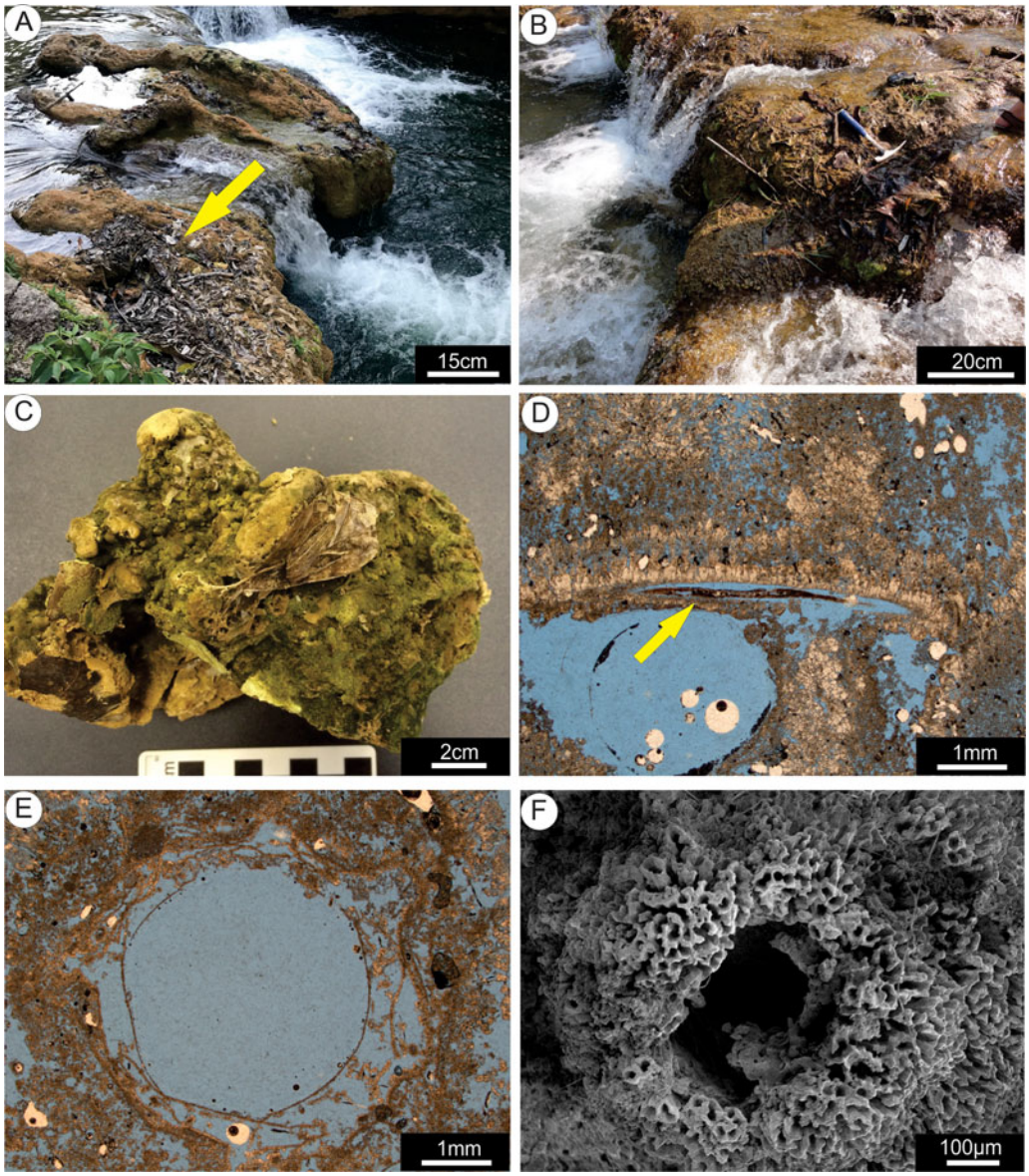

Figure 5. Phytoclastic rudstone. (A) Dam formed by the accumulation of leaves and plant fragments (yellow arrow). (B) Phytoclasts deposited at the top of a dam. (C) Uncoated plant fragments in a greenish micritic matrix. (D) Microscope image; phytoclast with organic matter preserved (yellow arrow) calcified with clear spar crystals. (E) Phytoclast covered by micrite to microspar crystals; note the moldic porosity. (F) SEM image; plant stalk with a diameter of 25 µm, covered by calcite and associated with small calcified tubes.

Porosity interpretation

The characterization of porosity using micro-CT predominantly revealed primary and selective types of pores, indicating that the arrangement of components is primarily influenced by depositional events. It is important to note that the remarkably high values of total porosity observed in all tufa facies are due to limited compaction and minimal burial influence (Oste et al., 2023). Diagenetic features that typically reduce porosity, such as cementation and aggrading neomorphism, are minimal in active tufa facies (Oste et al., 2023) and have negligible effects on the overall pore volume and connectivity.

Mineralogical, chemical, and isotopic results

The 25 samples were analyzed using XRD (X-ray diffraction) (Fig. 7A) and XRF (X-ray fluorescence) (Fig. 7B) techniques to obtain geochemical results. The samples were classified into four facies, and the mean values of semi-quantitative mineralogical results, major oxides, and volatiles were calculated for each facies group. Minor oxides, such as Na_2O, K_2O, TiO_2, MnO, and P_2O_5, comprised less than 0.5% of each sample and are not considered in the graph (Fig. 7).

The results of the chemical analysis indicated similar and frequent content of CaO and volatiles, including water, CO_2, and organic matter (volatiles obtained through lost on ignition [LOI]) across all tufa facies (Fig. 7B). Some samples exhibited an increase in silica concentration, contrasting with the depletion of CaO. The presence of aluminum silicates, likely clay minerals such as illite, was suggested by the correlation between increased Al_2O_3 and silica values. Chemical results obtained through XRF were confirmed by XRD analysis, which revealed that all samples were composed primarily of calcite (mean 96–98%) with occasional detrital quartz (mean 2–4%) (Fig. 7A).

https://doi.org/10.1017/qua.2024.26 Published online by Cambridge University Press

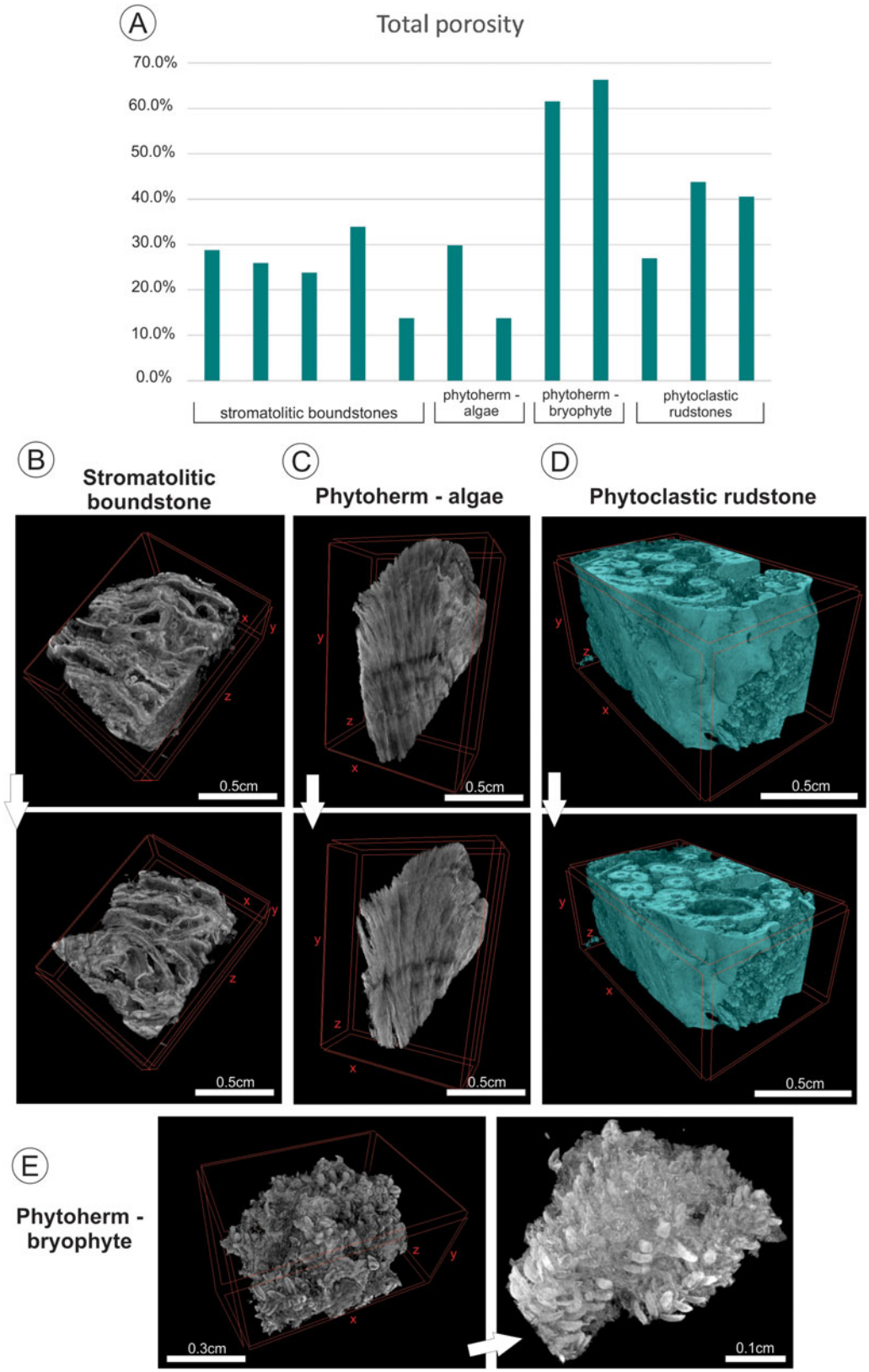

Figure 6. (A) Graph showing total porosity values; Note the high porosity values in the phytoherm boundstone of bryophytes. (B) Microtomographic images of the stromatolitic boundstone, which has fenestral pores aligned with the lamination; the arrow indicates a cut on the y-axis within the sample. (C) Microtomographic images of the phytoherm boundstone of algae, which has growth-framework porosity with pores between the filaments; the arrow indicates a cut on the z-axis within the sample. (D) Microtomographic images of the phytoclastic rudstone; the arrow indicates a cut on the y-axis within the sample. (E) Microtomographic images of the phytoherm boundstone of bryophyte, normally associated with moss leaves; the arrow indicates additional magnification of the sample.

https://doi.org/10.1017/qua.2024.26 Published online by Cambridge University Press

Table 1. Summary of total porosity, isolated pores, and open porosity for tufa samples of each facies

FACIES	Total porosity	Isolated pores	Open porosity
Stromatolitic boundstone	26.96%	0.67%	26.29%
Stromatolitic boundstone	43.80%	0.56%	43.24%
Stromatolitic boundstone	40.54%	0.35%	40.19%
Stromatolitic boundstone	61.56%	0.16%	61.39%
Stromatolitic boundstone	66.32%	0.16%	66.16%
Phytoherm – algae	29.81%	1.04%	28.77%
Phytoherm – algae	13.76%	1.74%	12.02%
Phytoherm – bryophyte	28.79%	0.80%	27.98%
Phytoherm – bryophyte	25.91%	1.24%	24.67%
Phytoclastic rudstone	23.81%	0.70%	23.11%
Phytoclastic rudstone	33.91%	0.58%	33.32%
Phytoclastic rudstone	13.77%	1.30%	12.48%

Isotopic analysis was conducted using 25 selected samples, which exhibited variations in $\delta^{18}O$ values ranging from −6.35 to −8.65‰ VPDB (average of −7.52‰ VPDB), and $\delta^{13}C$ values ranging from −6.16 to −9.52‰ VPDB (average of −8‰ VPDB). A positive correlation ($R^2 = 0.41$) was observed between the two isotopes across all samples (Fig. 8A). The $\delta^{18}O$ and $\delta^{13}C$ plot by facies (Fig. 8B) revealed that phytoherm boundstone of algae exhibited the lowest $\delta^{13}C$ values, while certain phytoclastic rudstones samples had the highest $\delta^{13}C$ values. Stromatolitic boundstones were scattered through the $\delta^{13}C$ range, and phytoherm boundstones of bryophytes displayed the most consistent $\delta^{18}O$ values.

Mineralogical, chemical, and isotopic interpretation

There are only two major chemical compounds in tufa samples: calcium, which forms calcite, and silica. Silica appears in freshwater tufa system as: (1) detrital quartz (Ribeiro et al., 2015), deposited into pools or dam environments, and is likely related to flooding events or windblown activity; (2) remains of diatom frustules; (3) vadose silt or clay infiltration in inactive tufa, related to pedogenetic processes; and (4) clay minerals, such as illite (aluminosilicate).

The highest values of SiO_2, normally associated with the presence of quartz, are observed in phytoclastic rudstones, indicating that detrital grains are transported with phytoclasts and deposited at the bottoms of pools. In contrast, the lowest SiO_2 values correspond to boundstones (stromatolites and phytoherm facies), which indicates an autochtonous process of tufa formation, without the presence of detrital grains.

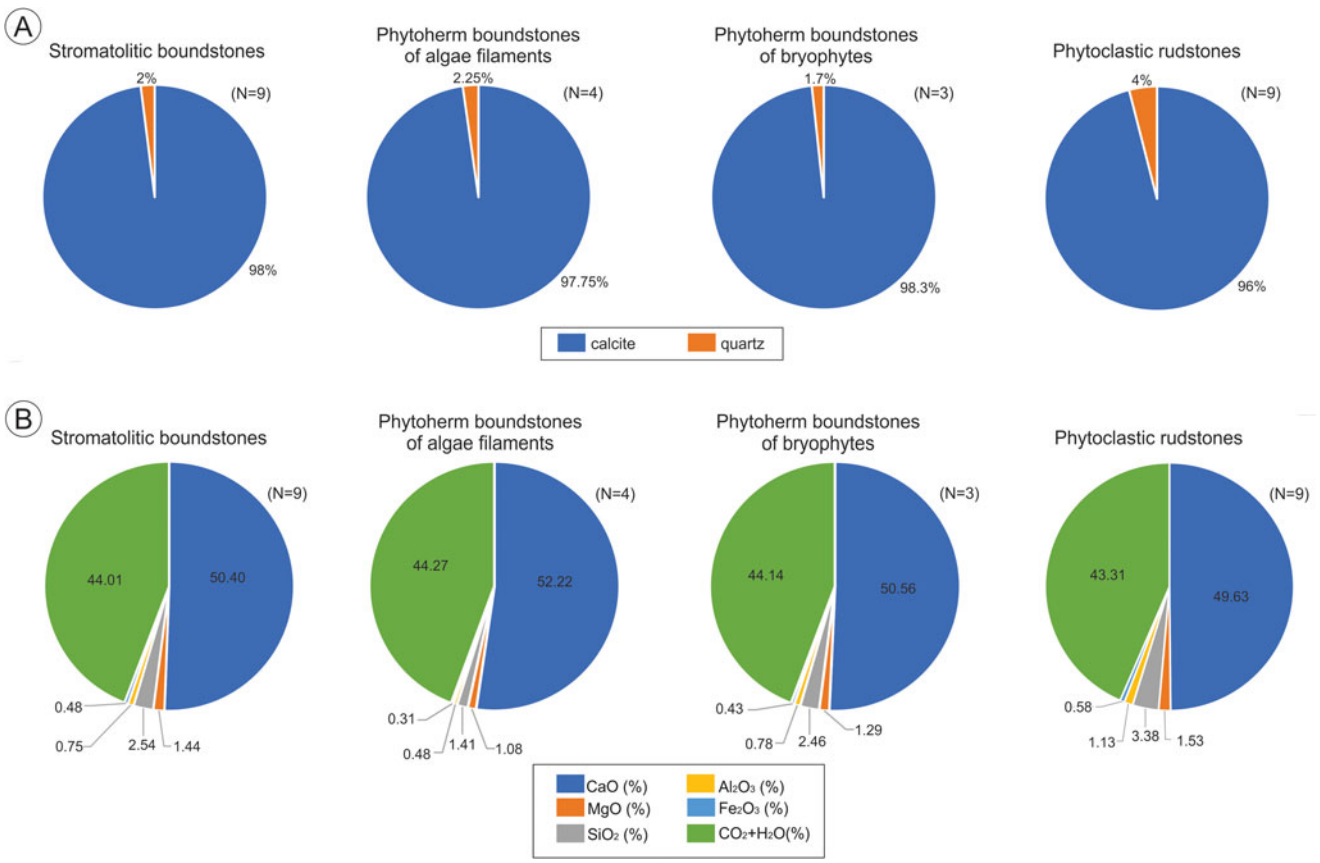

Figure 7. (A) XRD results by facies. (B) XRF results by facies. Minor oxides (< 0.5%) are not shown in the graphs.

https://doi.org/10.1017/qua.2024.26 Published online by Cambridge University Press

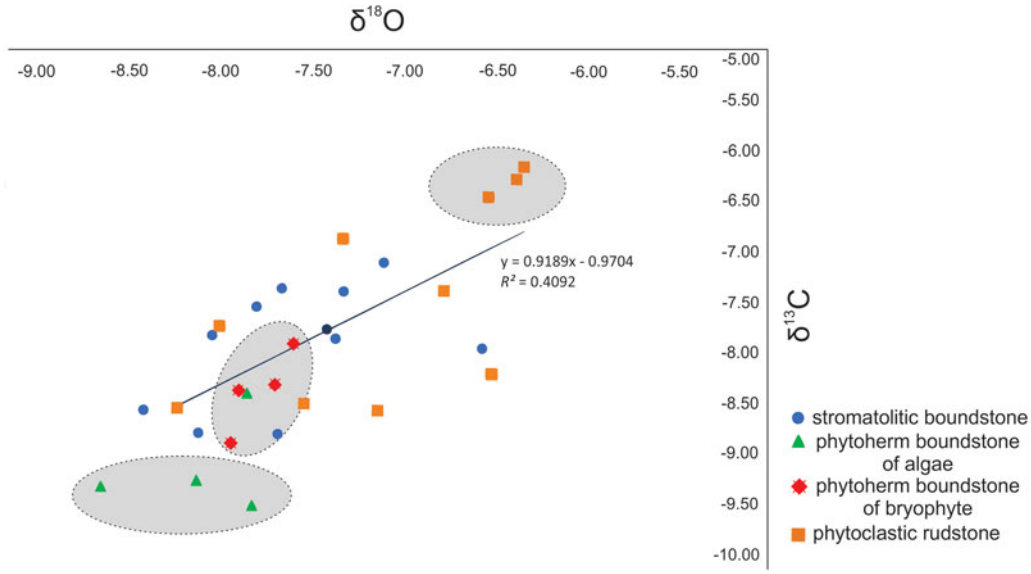

Figure 8. Cross plot of stable carbon and oxygen data for 25 selected samples. The $\delta^{18}O$ values range from −6.35 to −8.65‰ VPDB (average of −7.52‰ VPDB). The $\delta^{13}C$ values range from −6.16 to −9.52‰ VPDB (average of −8‰ VPDB). A positive correlation ($R^2 = 0.41$) is observed between the two isotopes. The dotted highlights indicate the phytoclastic boundstone of algae with the lowest $\delta^{13}C$ values (bottom), some samples of phytoclastic rudstone with the highest $\delta^{13}C$ values (top), and phytoherm boundstone of bryophyte with the most consistent $\delta^{18}O$ values (center).

The $\delta^{18}O$ value of meteoric water in Campo Grande City (near Bonito) is reported to be −7.36‰ VSMOW (Vienna Standard Mean Ocean Water), based on data from GNIP (Global Network for Isotopes in Precipitation) stations (Paula, 2012). A negative trend in $\delta^{18}O$ represents meteoric fluid with rainout effect (Andrews, 2006), which is consistent with the isotopic values of meteoric water in the region. The $\delta^{18}O$ values obtained in this study are similar to those reported by Boggiani et al. (2002).

Isotopic values of $\delta^{13}C$ are consistent with values from recent tufas around Bonito (Boggiani et al., 2002). Those values indicate influence of C3 plants and cyanobacteria (Schidlowski, 2000), along with possible contribution of streams and waterfalls coming from wooded areas where local groundwater contains isotopically light carbon. Some highly negative $\delta^{13}C$ values are also associated with groundwater enriched with light soil carbon (Andrews et al., 1997). The isotopic values of $\delta^{13}C$ correspond to forested lowland streams (Deocampo, 2010). Measurements of Bonito samples confirm the typical isotopic values for tufa systems ($\delta^{13}C$: −2 to −12‰ VPDB) (Pentecost, 1995; Özkul et al., 2013; Capezzuoli et al., 2014).

Discussion

Relation between microorganisms and $CaCO_3$ precipitation in different tufa facies

Recent freshwater tufa deposits are formed as a result of the interaction between physicochemical and biological processes (Pedley et al., 1996; Kano et al., 2003; Shiraishi et al., 2008a, 2010; Gradziński, 2010; Arenas et al., 2014a, 2015; Arenas and Jones, 2017). The primary cause of calcite supersaturation is the loss of CO_2, which occurs through two pathways: (1) a physicochemical process, where mechanical CO_2 outgassing, induced by water turbulence, leads to calcite precipitation; or (2) a biological process, involving photosynthesis. In fast-flowing waters, CO_2 outgassing typically occurs through the mechanical pathway due to water turbulence (Arenas et al., 2014a), whereas the photosynthetic process is more significant in slow-flowing waters or stagnant areas.

Generally, $CaCO_3$ precipitation in tufa deposits has been attributed to abiotic factors, primarily intense CO_2 degassing in fast-flowing waters. Biotic precipitation has been limited to areas with slow-flowing water, with extracellular polymeric substances (EPS) considered as nucleation sites for mineralization (Freytet and Plet, 1996; Merz-Preiß and Riding, 1999; Turner and Jones, 2005). However, recent studies have revealed the significance of microorganisms, particularly filamentous cyanobacteria, in tufa formation (Shiraishi et al., 2008a, b, 2010, 2017; Arp et al., 2010; Pedley, 2014), even in areas with rapid and turbulent flow. The surfaces of stromatolitic boundstones are densely colonized by cyanobacteria, which stimulates CO_2 uptake through photosynthesis, leading to an increase in the saturation state within the diffusive boundary layer and subsequent $CaCO_3$ precipitation. Studies have shown that during dark conditions, despite high fluid supersaturation, $CaCO_3$ precipitation ceases, indicating biologically induced mineralization driven by photosynthesis (Shiraishi et al., 2008a, 2010, 2017; Arp et al., 2010).

The Taika and Mimosa sites, both located in the Mimoso River, display a stepped longitudinal profile (Arenas-Abad et al., 2010) characterized by small waterfalls, cascades, and dam–pool–cascade environments (Oste et al., 2021). Tufa boundstones and rudstones were collected from these depositional systems, where sedimentation occurs under high $CaCO_3$ precipitation rates and mechanical CO_2 outgassing (Arenas et al., 2014a). Considering that the Mimoso River has intense mechanical CO_2 outgassing due to its stepped riverbed (Oste et al., 2021), the question arises regarding the actual relevance of biological processes in tufa formation and their effect on different facies (Fig. 9).

Previous research in the study area allowed recognition of a diverse community of microorganisms formed by filamentous algae (*Oocardium stratum* and *Vaucheria geminata*),

https://doi.org/10.1017/qua.2024.26 Published online by Cambridge University Press

Figure 9. Schematic diagram with the pool–barrage–cascade depositional subenvironment, the distribution of tufa facies, and the main process related to the formation of each facies.

cyanobacteria (*Phormidium incrustatum*), filamentous fungi, and pennate diatoms (Oste et al., 2018, 2021). Among the phototrophs observed in the stromatolites of Bonito, those containing abundant carboxyl groups within EPS, such as *Phormidium* and *Leptolyngbya*, were considered controllers of $CaCO_3$ nucleation (Shiraishi et al., 2022). According to Shiraishi et al. (2022), within well-developed biofilms of stromatolitic and laminated tufa, the $CaCO_3$ precipitation is induced by photosynthesis; nevertheless, abiotic precipitation remains the major process for tufa formation outside the biofilm (Shiraishi et al., 2022).

Stromatolitic boundstones are formed by an intercalation of micritic laminae and fibro-radiated laminae, which are influenced by seasonal changes in physicochemical conditions and/or microbial communities (Kano et al., 2003; Arenas et al., 2010, 2014a; Arenas and Jones, 2017). In the studied area, stromatolitic lamination is directly correlated with rainfall seasonality and, consequently, water discharge and microbial community preservation (Oste et al., 2021). Under SEM, microscopic facies of radiated tubes corresponding to *Oocardium stratum* (Chlorophyceae) (Golubić et al., 2008; Gradziński, 2010; Rott et al., 2010, 2012)

https://doi.org/10.1017/qua.2024.26 Published online by Cambridge University Press

are encrusted with trigonal-shaped calcitic mesocrystals (Oste et al., 2021). These tubes are covered by thick sheets of EPS, confirming biologically induced mineralization (Dupraz et al., 2009).

In laminated tufas in fast-flowing waters, there is an intrinsic relation among micrite, spar crystals, and EPS (Pedley, 2014). Within the EPS, or intra-EPS, precipitation of calcite is controlled by the external calcium ion supply and the biofilm, which produces small calcite crystals. In contrast, outside the EPS, the high ion supply favors the crystallization of well-organized calcite crystals (Pedley, 2014). According to Oste et al. (2021), a crystallization sequence occurs around tubes of *Oocardium stratum*: small crystals form around the filament within the EPS, while well-developed crystals such as rhombs (Fig. 3F) form outside the influence of EPS (extra-EPS). Although *Oocardium stratum* does not control the mineralization around the tubes, it accelerates the calcite precipitation (Tran et al., 2019).

Stromatolitic tufa develops in areas with both fast-flowing and slow-flowing water (Arenas-Abad et al., 2010; Gradziński et al., 2013), with intense calcite precipitation in the former due to rapid mechanical CO_2 outgassing and enhanced microbial activity, such as photosynthesis, in the slow-flowing water areas. Thus, the formation of stromatolitic boundstones results from the combined influences of inorganic and microbial factors on mineralization.

Phytohermal boundstones of bryophytes are formed in splash-water zones, with thin water laminae (Arenas-Abad et al., 2010; Gradziński et al., 2013). Calcite precipitation around mosses primarily occurs through a mechanical process, driven by the high supersaturation of the splashed water. These boundstones with bryophytes exhibit calcite precipitation around the moss leaves, indicating nucleation within a biofilm and subsequent progressive calcite encrustation via an inorganic pathway. SEM images confirm the precipitation of micrite around bryophytes, with limited or no detectable EPS remnants. These findings, which are supported by Shiraishi et al. (2008b), revealed that the contributions of other phototrophs, such as diatoms and mosses, are much less significant on biotic precipitation compared to filamentous cyanobacteria.

Phytohermal boundstones of algae are the main facies that reflects the intense biological process of precipitation. This facies forms in stagnant waters, such as pools and small ponds (Arenas-Abad et al., 2010), where mechanical CO_2 outgassing is minimal. Preserved algal mats exhibit *Oocardium stratum* filaments encrusted with calcitic mesocrystals characterized by trigonal shapes, which are typically associated with microorganisms (Turner and Jones, 2005; Spadafora et al., 2010; Manzo et al., 2012; Jones, 2017). Consequently, biotic activity is considered the principal process driving precipitation in these facies.

Phytoclastic rudstones, consisting of plant fragments, are typically deposited in calm areas, often at the tops of barriers, cascades, or in dammed conditions (Arenas-Abad et al., 2010; Vázquez-Urbez et al., 2012). Slow-flowing waters facilitate the preservation of algal and/or cyanobacterial filaments, contributing to tufa formation. The micrite encrustation of phytoclasts primarily occurs as an inorganic process, although cyanobacterial filaments, which can induce biotic precipitation, are common in the phytoclastic rudstones. Therefore, phytoclastic rudstones result from an interaction between mechanical and biological processes of mineralization.

The micro-CT characterization of porosity predominantly revealed primary and selective pore types, providing insights into the arrangement of components primarily influenced by depositional events. Boundstones of algae and stromatolites have the lowest rates of total porosity, due to a close fabric. Growth-framework porosities, which are formed between microbial filaments, occur extensively in both facies, indicating a biological influence on porosity development. In contrast, bryophytes and phytoclastic have the highest porosities, which are formed mainly by rapid calcite encrustation of molds of leaves and plant fragments. The micro-CT results contribute to a comprehensive understanding of porosity types, revealing the interplay between mechanical processes and biological influence in shaping the porosity characteristics within the studied tufa facies.

Isotopic signature due to microbial influence

The isotopic composition of freshwater tufa can be related to the environment and CO_2 degassing. Mechanical CO_2 degassing is more pronounced in areas with turbulent flow, such as waterfalls and cascades, leading to rapid calcite precipitation. This is reflected in higher $\delta^{13}C$ values compared to slow-flowing water areas (Arenas et al., 2007). However, there are several factors that can affect this correlation, including the influence of underground and surface water, variations in flow conditions, water velocity, changes in soil CO_2 contributions, biological activity, photosynthesis, degree of CO_2 degassing, and isotopic composition of the parental rock (Andrews, 2006; Arenas-Abad et al., 2010).

In our study, we did not observe a clear trend between the carbon isotope ratios of tufa facies and water velocity, suggesting that other factors are influencing the isotopic composition. These factors may include rainfall patterns, the contribution of C3 and C4 plants, and the uptake of $^{12}CO_2$ by cyanobacteria in stromatolites (Schidlowski, 2000; Arenas-Abad et al., 2010).

Photosynthesis is associated with the preferential uptake of $^{12}CO_2$, leading to an enrichment of ^{13}C in dissolved inorganic carbon (DIC) and, subsequently, in the precipitated carbonate. However, the magnitude of this enrichment does not significantly affect the overall carbon distribution, which can vary depending on the environment and the types of plants present (Andrews et al., 2000). The $\delta^{13}C$ enrichment due to photosynthesis is particularly more significant in microenvironments dominated by algae and cyanobacteria (Arp et al., 2001), which is evident in the most-negative $\delta^{13}C$ values that were observed in boundstones of algae in our study. Negative $\delta^{13}C$ values in these boundstones may imply that the uptake of light ^{12}C from mosses and algae combines with the signal originating from soil sources.

Isotopic $\delta^{13}C$ values do not appear to distinguish between induced or influenced microbial precipitation. This lack of differentiation is attributed to the absence of enzymatic fractionation of carbon isotopes associated with microbial respiration or photosynthesis in these processes (Della Porta, 2015). Although the $\delta^{13}C$ signature in tufa does not accurately indicate a direct correlation between microbial precipitation and the presence of biological activity, it also does not necessarily imply that the precipitation is exclusively inorganic (Shiraishi et al., 2008b).

More-negative isotopic $\delta^{18}O$ values primarily indicate a meteoric fluid with rainout effect (Andrews, 2006). Laminated tufa is commonly used in several paleoclimatic studies (Andrews, 2006; Arenas et al., 2010; Arenas and Jones, 2017), where there is typically a good correlation between $\delta^{18}O$ values and seasonal changes in water temperature. In our work, we were unable to identify any significant climatic change, only confirming the meteoric origin of the fluid and minimal influence from intense

https://doi.org/10.1017/qua.2024.26 Published online by Cambridge University Press

evaporation, owing to the typical climate in the region with high annual precipitation.

The observed negative trend in $\delta^{13}C$ and $\delta^{18}O$ within tufas from the Bonito region aligns with the typical range found in calcareous tufa deposits globally (Pentecost, 2005). The effect of diagenesis on recent tufa deposits from Bonito appears to be minimal (Oste et al., 2023), suggesting that, besides the tufa formation being regarded as an open system, the isotopic signal is closely related to the original precipitation conditions. It is noteworthy that the $\delta^{13}C$ isotopic composition incorporates contributions of various local-scale fractionation processes (Arenas et al., 2010). The primary factors contributing to the $\delta^{13}C$ and $\delta^{18}O$ signatures include mechanical outgassing of CO_2, the presence of light CO_2 derived from soil, biological activity within facies rich in moss and algae, and input from meteoric sources.

Conclusions

Six conclusions emerge based on the facies and geochemical analysis conducted in this study. (1) The formation of stromatolitic boundstones is influenced by both biotic and abiotic processes. The presence of *Oocardium stratum* and EPS filaments indicates the involvement of microbial activity, while rapid CO_2 degassing plays a significant role in mineralization in fast-flowing waters. (2) Calcite precipitation around mosses in phytohermal boundstones of bryophytes is primarily driven by a mechanical process due to the high supersaturation of splashed water. In boundstones of algae, biotic activity is identified as the principal precipitation-driving process. The formation of phytoclastic rudstones results mainly from a mechanical process, although the presence of microorganisms is common and may influence the precipitation. (3) Porosity varies among different tufa facies. Stromatolites and phytoherm boundstones of algae exhibit lower porosity due to their compact fabric, whereas phytoherm boundstones of bryophytes and phytoclastic rudstones display higher porosity resulting from intense and rapid encrustation of phytoclasts and mosses. (4) The presence of calcified tubes of *Oocardium stratum* and abundant EPS associated with trigonal calcitic crystals strongly supports the biogenic-influenced origin of tufas, even in turbulent environments. (5) The isotopic composition of freshwater tufa in the Bonito region is influenced by CO_2 outgassing and environmental factors, such as water sources and flow conditions. The negative trend of $\delta^{13}C$ is likely attributed to photosynthetic processes and the contribution of light carbon-enriched groundwater. (6) Photosynthesis contributes to isotopic enrichment, particularly in microenvironments dominated by algae and cyanobacteria, as evinced by the lighter isotopic values of phytoherm boundstones of algae. However, it is important to note that the isotopic composition does not always directly correlate with photosynthesis. These findings enhance our understanding of the influence of microorganisms on tufa formation and highlight the complex interplay between biotic and abiotic processes in the development of different tufa facies.

Acknowledgments. We wish to thank INPEX Corporation, especially Dr. Jiro Asada, for the fomentation of this work, including financial support for field trips and laboratory analyses. We also thank all the colleagues and professionals of LAMIR at Universidade Federal do Paraná. We are pleased to acknowledge Dr. Fumito Shiraishi and his students at Hiroshima University for the support and all the constructive comments. This paper is based on a master's study conducted at Universidade Federal do Paraná that was supported by the Geobiocal Project/LAMIR and University of Hiroshima.

References

Almeida F.F.M., 1965. Geologia da Serra da Bodoquena (Mato Grosso). *DNPM/DGM Boletim* **219**, 96 pp.

Alvarenga, C.J.S., Trompette R., 1993. Evolução tectônica Brasiliana da Faixa Paraguai: a estruturação da região de Cuiabá. *Revista Brasileira de Geociências* **23**, 18–30.

Andrews, J.E., 2006. Paleoclimatic records from stable isotopes in riverine tufas: synthesis and review. *Earth-Science Reviews* **75**, 85–104.

Andrews, J.E., Brasier, A.T., 2005. Seasonal records of climatic change in annually laminated tufas: short review and future prospects. *Journal of Quaternary Science* **20**, 411–421.

Andrews, J.E., Riding, R, Dennis, P.F., 1997. The stable isotope record of environmental and climatic signals in modern terrestrial microbial carbonates from Europe. *Palaeogeography, Palaeoclimatology, Palaeoecology* **129**, 171–189.

Andrews, J.E., Pedley, H.M., Dennis, P.F., 2000. Paleoenvironmental records in Holocene Spanish tufas: a stable isotope approach in search of reliable climatic archives. *Sedimentology* **47**, 961–978.

Arenas, C., Jones, B., 2017. Temporal and environmental significance of microbial lamination: Insights from Recent fluvial stromatolites in the River Piedra, Spain. *Sedimentology* **64**, 1597–1629.

Arenas, C., Cabrera, L., Ramos, E., 2007. Sedimentology of tufa facies and continental microbialites from the Palaeogene of Mallorca Island (Spain). *Sedimentary Geology* **197**, 1–27.

Arenas, C., Osácar, C., Sancho, C., Vázquez-Urbez, M., Auqué, L., Pardo, G., 2010. Seasonal record from recent fluvial tufa deposits (Monasterio de Piedra, NE Spain): sedimentological and stable isotope data. In: Yoshida, M., Windley, B.F., Dasgupta, S. (Eds.), *Tufas and Speleothems: Unravelling the Microbial and Physical Controls*. Geological Society, London, Special Publications **336**, p. 119–142.

Arenas, C., Vázquez-Urbez, M., Auqué, L., Sancho, C., Osácar, C., Pardo, G., 2014a. Intrinsic and extrinsic controls of spatial and temporal variations in modern fluvial tufa sedimentation: a thirteen-year record from a semi-arid environment. *Sedimentology* **61**, 90–132.

Arenas, C., Vázquez-Urbez, M., Pardo. G., Sancho, C., 2014b. Sedimentology and depositional architecture of tufas deposited in stepped fluvial systems of changing slope: Lessons from the Quaternary Añamaza valley (Iberian Range, Spain). *Sedimentology* **61**, 133–171.

Arenas, C., Piñuela, L., García-Ramos, J.C., 2015. Climatic and tectonic controls on carbonate deposition in syn-rift siliciclastic fluvial systems: a case of microbialites and associated facies in the Late Jurassic. *Sedimentology* **62**, 1149–1183.

Arenas-Abad, C., Vázquez-Urbez, M., Pardo-Tirapu, G., Sancho-Marcén, C., 2010. Fluvial and associated carbonate deposits. In: Alonso-Zarza, A.M., Tanner, L.H. (Eds.), *Carbonates in Continental Settings: Facies, Environments and Processes*. Developments in Sedimentology **61**, 133–175.

Arp, G., Reimer, A., Reitner, J., 2001. Photosynthesis-induced biofilm calcification and calcium concentrations in Phanerozoic oceans. *Science* **292**, 1701–1704.

Arp, G., Bissett, A., Brinkmann, N., Cousin, S., De Beer, D., Friedl, T., Mohr, K.I., *et al.*, 2010. Tufa-forming biofilms of German karstwater streams: microorganisms, exopolymers, hydrochemistry and calcification. In: Pedley, H.M., Rogerson, M. (Eds.), *Tufas and Speleothems: Unravelling the Microbial and Physical Controls*. Geological Society, London, Special Publications **336**, 83–118.

Berrendero, E., Arenas, C., Mateo, P., Jones, B., 2016. Cyanobacterial diversity and related sedimentary facies as a function of water flow conditions: example from the Monasterio de Piedra Natural Park (Spain). *Sedimentary Geology* **337**, 12–28.

Boggiani, P.C., Fairchild, T.R., Coimbra, A.M., 1993. O Grupo Corumbá (Neoproterozóico–Cambriano) na região central da Serra da Bodoquena (Faixa Paraguai), Mato Grosso do Sul. *Revista Brasileira de Geociências* **23**, 301–305.

Boggiani, P.C., Coimbra, A.M., Gesicki, A.L.D., Sial, A.N., Ferreira, V.P., Ribeiro, F.B., Flexor, J.M., 2002. Tufas Calcárias da Serra da Bodoquena,

https://doi.org/10.1017/qua.2024.26 Published online by Cambridge University Press

MS. In: Schobbenhaus, C., Campos, D.A., Queiroz, E.T., Winge, M, Berbert-Born, M.L.C. (Eds.) *Sítios Geológicos e Paleontológicos do Brasil*. DNPM, Brasília, pp. 249–259.

Boggiani, P.C., Alvarenga, C.J.S., 2004. Faixa Paraguai. In: Mantesso-Neto, V., Bartorelli, A., Carneiro, A.D.R., Brito-Neves, B.B. (Eds.) *Geologia do Continente Sul-Americano: Evolução da Obra de Fernando Flávio Marques de Almeida*. Beca Editora, São Paulo, pp. 113–121.

Campanha, G.A.C., Sallun Filho, W., Zuquim, M.P.S., 2011. A Faixa de Dobramento Paraguai na Serra da Bodoquena e Depressão do Rio Miranda, Mato Grosso do Sul. *Revista do Instituto de Geociências – USP* **11**, 79–96.

Capezzuoli, E., Gandin, A., Pedley, M., 2014. Decoding tufa and travertine (fresh water carbonates) in the sedimentary record: the state of the art. *Sedimentology* **61**, 1–21.

Choquette, P.W., Pray, L.C., 1970. Geologic nomenclature and classification of porosity in sedimentary carbonates. *The American Association of Petroleum Geologists Bulletin* **54**, 207–250.

Della Porta, G., 2015. Carbonate build-ups in lacustrine, hydrothermal and fluvial settings: comparing depositional geometry, fabric types and geochemical signature. In: Bosence, D.W.J., Gibbons, K.A., Le Heron, D.P., Morgan, W.A., Pritchard, T., Vining, B.A. (Eds.), *Microbial Carbonates in Space and Time: Implications for Global Exploration and Production*. Geological Society, London, Special Publications **418**, 17–68. https://doi.org/10.1144/sp418.4.

Deocampo, D.M., 2010. The geochemistry of continental carbonates. In: Alonso-Zarza, A.M., Tanner, L.H. (Eds.). *Carbonates in Continental Settings: Geochemistry, Diagenesis and Applications*. Elsevier, Amsterdam, pp. 1–59.

Dunham, R.J., 1962. Classification of carbonate rocks according to depositional texture. In: Ham, W.E. (Ed.) *Classification of Carbonate Rocks*. American Association of Petroleum Geologists, Memoir **1**, pp. 108–122.

Dupraz, C., Reid, R.P., Braissant, O., Decho, A.W., Norman, R.S., Visscher, P.T., 2009. Processes of carbonate precipitation in modern microbial mats. *Earth-Science Reviews* **96**, 141–162.

Embry, A.F., Klovan, J.E., 1971. A Late Devonian reef tract on northeastern Banks Islands, Northwest Territories. *Bulletin of Canadian Petroleum Geology* **19**, 730–781.

Ford, T.D., Pedley, H.M., 1996. A review of tufa and travertine deposits of the world. *Earth Science Reviews* **41**, 117–175.

Freytet, P., Plet, A., 1996. Modern freshwater microbial carbonates: the *Phormidium* stromatolites (tufa–travertine) of southeastern Burgundy (Paris Basin, France). *Facies* **34**, 219–238.

Golubić, S., Violante, C., Plenkovic-Moraj, A., Grgasovic, T., 2008. Travertines and calcareous tufa deposits: an insight into diagenesis. *Geologia Croatica* **61**, 363–378.

Gradziński, M., 2010. Factors controlling growth of modern tufa: results of a field experiment. In: Pedley, H.M., Rogerson, M. (Eds.), *Tufas and Speleothems: Unravelling the Microbial and Physical Controls*. Geological Society of London, Special Publications **336**, 143–191.

Gradziński, M., Hercman, H., Jaskiewicz, M., Szczurek, S., 2013. Holocene tufa in the Slovak Karst: facies, sedimentary environments and depositional history. *Geological Quarterly* **57**, 769–788.

Jones, B., 2017. Review of aragonite and calcite crystal morphogenesis in thermal spring systems. *Sedimentary Geology* **354**, 9–23.

Kano, A., Matsuoka, J., Kojo, T., Fujii, H., 2003. Origin of annual laminations in tufa deposits, southwest Japan. *Paleogeography, Paleoclimatology, Paleoecology* **191**, 243–262.

Manzo, E., Perri, E., Tucker, M.E., 2012. Carbonate deposition in a fluvial tufa system: processes and products (Corvino Valley – southern Italy). *Sedimentology* **59**, 553–577.

Merz-Preiß, M., Riding, R., 1999. Cyanobacterial tufa calcification in two freshwater streams: ambient environment, chemical thresholds and biological processes. *Sedimentary Geology* **126**, 103–124.

Oliveira, E.C., Rossetti, D.F., Utida, G., 2017. Paleoenvironmental evolution of continental carbonates in west-central Brasil. *Anais da Academia Brasileira de Ciências* **89**, 407–429.

Oste, J.T.F., Arai, M., França, A.B., Cury, L.F., Bahniuk, A.M., 2018. Geoquímica e palinologia de tufas calcárias da região de Bonito (MS): implicações ambientais. *Geociências* **37**, 733–744.

Oste, J.T.F., Rodríguez-Berriguete, A., Dal'Bó, P.F., 2021. Depositional and environmental controlling factors on the genesis of Quaternary tufa deposits from Bonito region, Central-West Brazil. *Sedimentary Geology* **413**, 105824. https://doi.org/10.1016/j.sedgeo.2020.105824.

Oste, J.T.F., Rodríguez-Berriguete, A., Dal'Bó, P.F., 2023. Coarsening of tufa textures through early diagenesis: modern and fossil examples from Bonito region (Central-West, Brazil). *Journal of South American Earth Sciences* **128**, 104450. https://doi.org/10.1016/j.jsames.2023.104450.

Özkul, M., Kele, S., Gökgöz, A., Shen, C., Jones, B., Baykara, M.O., Fórizs, I., Németh, T., Chang, Y., Alçiçek, M.C., 2013. Comparison of the Quaternary travertine sites in the Denizli extensional basin based on their depositional and geochemical data. *Sedimentary Geology* **294**, 179–204.

Paula, M.S., 2012. Variabilidade do Sistema de monções de verão durante os últimos 1500 anos na região de Bonito – MS, com base em registros paleoclimáticos de espeleotemas. Master's thesis, Instituto de Geociências, Universidade de São Paulo, São Paulo, 121 pp.

Pedley, M., 2014. The morphology and function of thrombolytic calcite precipitating biofilms: a universal model derived from freshwater mesocosm experiments. *Sedimentology* **61**, 22–40.

Pedley, M., Andrews, J., Ordonez, S., Garcia del Cura, M.A., Martin, J.A.G., Taylor, D., 1996. Does climate control the morphological fabric of freshwater carbonates? A comparative study of Holocene barrage tufas from Spain and Britain. *Paleogeography, Paleoclimatology, Paleoecology* **121**, 239–257.

Pedley, M., Rogerson, M., Middleton, R., 2009. Freshwater calcite precipitates from in vitro mesocosm flume experiments: a case for biomediation of tufas. *Sedimentology* **56**, 511–527.

Pentecost, A., 1995. The Quaternary travertine deposits of Europe and Asia Minor. *Quaternary Science Reviews* **14**, 1005–1028.

Pentecost, A., 2005. *Travertine*. Springer, Berlin.

Ribeiro, L.M.A.L., Sawakuchi, A.O., Wang, H., Sallun Filho, W., Nogueira, L., 2015. OSL dating of Brazilian fluvial carbonates (tufas) using detrital quartz grains. *Quaternary International* **362**, 146–156.

Riccomini, C., Nogueira, A.C.R., Sial, A.N., 2007. Carbon and oxygen isotope geochemistry of Ediacaran outer platform carbonates, Paraguay Belt, central Brazil. *Anais da Academia Brasileira de Ciências* **79**, 519–527.

Riding, R., 1991. Classification of microbial carbonates. In: Riding, R. (Ed.), *Calcareous Algae and Stromatolites*. Springer-Verlag, Berlin, pp. 21–51.

Riding, R., 2000. Microbial carbonates: the geological record of calcified bacterial-algal mats and biofilms. *Sedimentology* **47**, 179–214.

Romero, G.R., Sanchez, E.A.M., Morais, L., Boggiani, P.C., Fairchild, T.R., 2016. Tubestone microbialite association in the Ediacaran cap carbonates in the southern Paraguay Fold Belt (SW Brazil): geobiological and stratigraphic implications for a Marinoan cap carbonate. *Journal of South American Earth Sciences* **71**, 172–181.

Rott, E., Holzinger, A., Gesierich, D., Kofler, W., Sanders, D., 2010. Cell morphology, ultrastructure, and calcification pattern of *Oocardium stratum*, a peculiar lotic desmid. *Protoplasma* **243**, 39–50.

Rott, E., Hotzy, R., Cantonati, M., Sanders, D., 2012. Calcification types of *Oocardium stratum* Nägeli and microhabitat conditions in springs of the Alps. *Freshwater Science* **31**, 610–624.

Sallun Filho, W., 2005. Geomorfologia e Geoespeleologia dos Carste da Serra da Bodoquena, MS. Doctoral thesis, Instituto de Geociências, Universidade de São Paulo, São Paulo, 216 pp.

Sallun Filho, W., Karmann, I., Boggiani, P.C., Petri, S., Cristalli, P.S., Utida, G., 2009a. A deposição de tufas Quaternárias no Estado de Mato Grosso do Sul: proposta de definição da Formação Serra da Bodoquena. *Revista do Instituto de Geociência – USP* **9**, 47–60.

Sallun Filho, W., Karmann, I., Sallun, A.E.M., Suguio, K., 2009b. Quaternary tufa in the Serra da Bodoquena Karst, West-Central Brazil: evidence of wet period. *IOP Conf. Series: Earth and Environmental Science* **6**, 072055. https://doi.org/10.1088/1755-1307/6/7/072055.

Schidlowski, M., 2000. Carbon isotopes and microbial sediments. In: Riding, R.E., Awramik S.M. (Eds.), *Microbial Sediments*. Springer-Verlag, Berlin, pp. 84–95.

Shiraishi, F., 2011. Photosynthesis-induced stromatolite formation in the freshwater creeks. In: Reitner, J., Queric, N., Arp., G. (eds.) *Advances in Geobiology of Stromatolite Formation. Lecture Notes in Earth Sciences* **131**, pp. 135–140.

https://doi.org/10.1017/qua.2024.26 Published online by Cambridge University Press

Shiraishi, F., Bissett, A., de Beer, D., Reimer, A., Arp, G., 2008a. Photosynthesis, respiration and exopolymer calcium-binding in biofilm calcification (Westerhöfer and Deinschwanger Creek, Germany). *Geomicrobiology Journal* **25**, 83–94.

Shiraishi, F., Reimer, A., Bissett, A., de Beer, D., Arp, G., 2008b. Microbial effects on biofilm calcification, ambient water chemistry and stable isotope records in a highly supersaturated setting (Westerhöfer Bach, Germany). *Paleogeography, Paleoclimatology, Paleoecology* **262**, 91–106.

Shiraishi, F., Okumura, T., Takahashi, Y., Kano, A., 2010. Influence of microbial photosynthesis on tufa stromatolite formation and ambient water chemistry, SW Japan. *Geochimica et Cosmochimica Acta* **74**, 5289–5304.

Shiraishi, F., Hanzawa, Y., Okumura, T., Tomioka, N., Kodama, Y., Suga, H., Takahashi, Y., Kano, A., 2017. Cyanobacterial exopolymer properties differentiate microbial carbonate fabrics. *Scientific Reports* **7**, 11805. https://doi.org/10.1038/s41598-017-12303-9.

Shiraishi, F., Hanzawa, Y., Asada, J., Cury, L.F., Bahniuk, A.M., 2022. Microbial influences on tufa deposition in a tropical climate. *Sedimentary Geology* **427**, 106045. https://doi.org/10.1016/j.sedgeo.2021.106045.

Spadafora, A., Perri, E., Mckenzie, J.A., Vasconcelos, C., 2010. Microbial biomineralization processes forming modern Ca:Mg carbonate stromatolites. *Sedimentology* **57**, 27–40.

Tran, H., Rott, E., Sanders, D., 2019. Exploring the niche of a highly effective biocalcifier: calcification of the eukaryotic microalga *Oocardium stratum* Nägeli 1849 in a spring stream of the Eastern Alps. *Facies* **65**, 37. https://doi.org/10.1007/s10347-019-0578-z.

Turner, E.C., Jones, B., 2005. Microscopic calcite dendrites in cold-water tufa: implications for nucleation of micrite and cement. *Sedimentology* **52**, 1043–1066.

Utida, G., Petri, S., Oliveira, E.C., Boggiani, P.C., 2012. Microfossils in micrites from Serra da Bodoquena (MS), Brazil: taxonomy and paleoenvironmental implications. *Anais da Academia Brasileira de Ciências* **84**, 245–261.

Utida, G., Oliveira, E.C., Tucker, M., Petri, S., Boggiani, P.C., 2017. Palaeoenvironmental interpretations based on molluscs from mid-Holocene lacustrine limestones, Mato Grosso do Sul, Brazil. *Quaternary International* **437**, 186–198.

Vásquez-Urbez, M., Arenas, C., Pardo, G., 2012. A sedimentary facies model for stepped, fluvial tufa systems in the Iberian Range (Spain): the Quaternary Piedra and Mesa valleys. *Sedimentology* **59**, 502–526.

https://doi.org/10.1017/qua.2024.26 Published online by Cambridge University Press